On an Improved State Parametrization for Soft Robots With Piecewise Constant Curvature and Its Use in Model Based Control

Cosimo Della Santina, Antonio Bicchi, and Daniela Rus

***Abstract*—Piecewise constant curvature models have proven to be an useful tool for describing kinematics and dynamics of soft robots. However, in their three dimensional formulation they suffer from many issues limiting their range of applicability - as discontinuities and singularities - mainly concerning the straight configuration of the robot. In this work we analyze these flaws, and we show that they are not due to the piecewise constant curvature assumption itself, but that instead they are a byproduct of the commonly employed direction/angle of bending parametrization of the state. We therefore consider an alternative state representation which solves all the discussed issues, and we derive a model based controller based on it. Examples in simulation are provided to support and describe the theoretical results. When using the novel parametrization, the system is able to perform more complex tasks, with a strongly reduced computational burden, and without incurring in spikes and discontinuous behaviors.**

***Index Terms*—Modeling, control, and learning for soft robots, motion control, natural machine motion.**

I. Introduction

In THE recent years, a growing attention has been devoted to developing controllers for continuum soft robots [1], namely robots made of continuously deformable soft materials [2]. While several important results have been obtained using the tools of machine learning [3], the use of model based control techniques has recently proven to be an effective alternative [4], [5]. In this context, piecewise constant curvature (PCC) models have proven to be a very useful tool with a vast range of applications. Examples include design [6], sensing [7], kinematic control [8], [9], feedforward dynamic control [10], feedback dynamic control [11], [12], just to cite a few. In a PCC model the soft robot is approximated as a sequence of continuous segments, with curvature constant in space (CC) but variable in time. Fig. 2(a) shows an example of a soft robot made of three CC segments.

Manuscript received August 12, 2019; accepted January 9, 2020. Date of publication January 17, 2020; date of current version January 30, 2020. This letter was recommended for publication by Associate Editor S. Coros and Editor K.-J. Cho upon evaluation of the reviewers' comments. This work was supported by the NSF under Grants Agreement NSF EFRI 1830901 and NSF 1226883. *(Corresponding author: Cosimo Della Santina.)*

C. Della Santina and D. Rus are with the Computer Science and Artificial Intelligence Laboratory, Massachusetts Institute of Technology, Cambridge, MA 02139 USA (e-mail: dsantina@mit.edu; rus@csail.mit.edu).

A. Bicchi is with the Research Center "E. Piaggio" and the Dept. of Information Engineering, University of Pisa, Pisa 56122, Italy and also with the "Soft Robotics for Human Cooperation and Rehabilitation" Lab, Istituto Italiano di Tecnologia, Genoa 16163, Italy (e-mail: antonio.bicchi@iit.it).

Digital Object Identifier 10.1109/LRA.2020.2967269

Despite the many accomplishments, PCC models have been regarded with suspicion by recent works in the field due to several issues they present, mainly concerning kinematic singularities and discontinuities [13]. These shortcomings can potentially produce critical behaviors in the practice, that we will discuss in detail in the letter.

More complex models - taking into account different kinds of strains - do not present these issues [13]–[16]. So it is a common belief in the field that the discussed problems are a product of the PCC hypothesis itself. We show here that this is actually a misconception, and that the issue lays instead in the parametrization of the robot configuration that has been historically used. This parametrization was introduced by the very first works proposing to use PCC assumption to manage the complexity of the continuum structure of the soft body [8], [17], [18].

In this work, we analyze the properties of a parametrization of the system state solving all the discussed issues, with specific focus on its use in model based control. The main intuition behind this parametrization comes from the observation of the classic rigid-bodied case. In rigid robots, the configuration is clearly connected to physical, directly measurable, quantities - i.e. the joint angles. This characteristics prevents the appearance of problems not directly concerning the physical nature of the system. We achieve the same in the soft case by considering as state of the robot a linear combination of lengths that can be directly measured on the robot structure.

In conclusion, this letter contributes with

- An in depth analysis of the main issues affecting the standard parametrization of 3D PCC models;
- A state parametrization, solving all the discussed issues;
- Simulations illustrating the theory.

II. The Standard Parametrization Does Not Define an Atlas of the Configuration Manifold

Consider a PCC robot composed of n segments with constant curvature (CC) connected in series, as exemplified in Fig. 2(a). We introduce n reference frames $\{S_1\}, \dots, \{S_n\}$ attached at the ends of each segment, plus one fixed base frame $\{S_0\}$. Under the PCC hypothesis, each segment is free to bend in any direction; its curvature is constant in space but variable in time; the segments are connected so that the resulting curve is everywhere differentiable. We consider here PCC soft robots for which also the length of each segment can change. Any other strain is neglected (see [18] for more details).

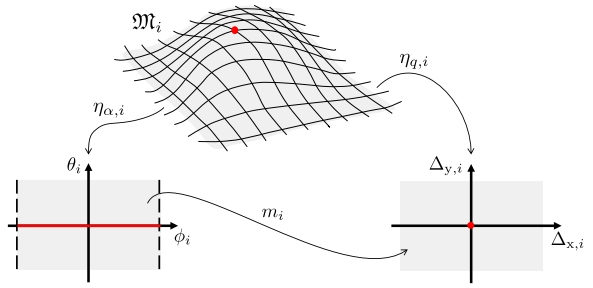

Fig. 1. The chart $\eta_{\alpha,i}$ classically used to describe the configuration manifold $\mathfrak{M}_i$ of a continuum soft segment with constant curvature generates artificial redundancies and singularities, which in turn produce pathological behaviors when controlling the robot. These characteristics are artificial in the sense that they are not a physical property of the system, but instead they are introduced by its mathematical description. In this work we analyze a set of coordinates $\Delta_{\mathrm{x},i}, \Delta_{\mathrm{y},i}$ alternative to the classic ϕ_i, θ_i. They are identified by a chart $\eta_{q,i}$ which we prove defining an atlas, i.e. it maps the whole $\mathfrak{M}_i$ one-to-one in the Euclidean space - solving the discussed issues. This reflects in strongly improved performance in simulating and controlling the robot.

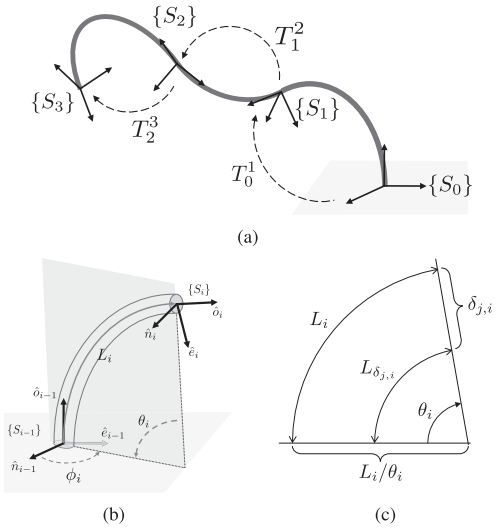

Fig. 2. Three views of PCC soft robots. Panel (a) shows a PCC soft robot made of three CC segments, and moving in three dimensions. The reference systems $\{S_i\}$ and the transformation matrices T^i_{i-1} are also reported in figure. Panel (b) depicts the i-th segment, with reference frames and α-parametrization highlighted. Panel (c) visually represents an arc at a distance $\delta_{j,i}$ from the axis along the direction of curvature.

We call $T^i_{i-1} \in \mathrm{SE}(3)$ the homogeneous transformation mapping $\{S_{i-1}\}$ into $\{S_i\}$

$$T^i_{i-1} = \begin{bmatrix} & R^i_{i-1} & & t^i_{i-1} \\ [0 & 0 & 0] & 1 \end{bmatrix}, \tag{1}$$

with $R^i_{i-1} = \begin{bmatrix}\{\hat{n}_i\}_{i-1} & \{\hat{e}_i\}_{i-1} & \{\hat{o}_i\}_{i-1}\end{bmatrix} \in \mathrm{SO}(3)$ rotation matrix, and $t^i_{i-1} \in \mathbb{R}^3$ translation. $\{\hat{n}_i\}_{i-1}, \{\hat{e}_i\}_{i-1}, \{\hat{o}_i\}_{i-1}$ are three unit vectors. They identify the three axes of $\{S_i\}$, with coordinates expressed w.r.t. $\{S_{i-1}\}$. It has been shown by Walker and colleagues in their seminal works on the topic [8], [17], that the manifold $\mathfrak{M}_i \subseteq \mathrm{SE}(3)$ in which T^i_{i-1} lives is of dimension three. Consequently the manifold $\mathfrak{M} = \mathfrak{M}_1 \times \cdots \times \mathfrak{M}_n$ has dimension 3n. To this end, they do not directly introduce a chart η_α from $\mathfrak{M}$ to $\mathbb{R}^{3n}$, as depicted in Fig. 1. They instead propose an inverse η_α^{-1} mapping, from $\mathbb{R}^{3n}$ to $\mathfrak{M}$. More specifically they introduce a parametrization $[\phi_i,\ \theta_i,\ \delta L_i]^{\mathrm{T}} \in \mathbb{R}^3$ for the

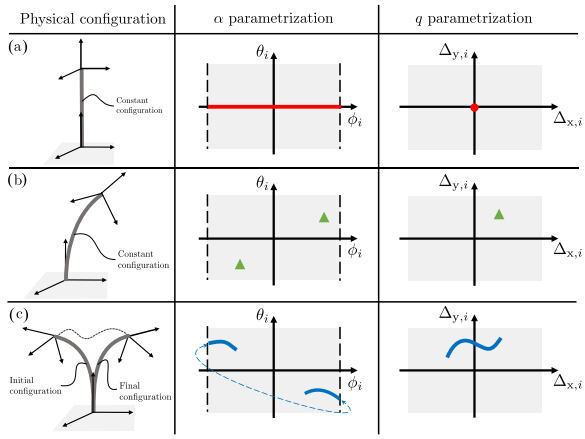

Fig. 3. Graphical representation of three shortcomings of the standard α parametrization. These problems occurring at the kinematic level reflects into major issues in the dynamic case. The q parametrization that we propose here is not affected by these flaws, as shown in the right part of the figure.

configuration of a segment (see Fig. 2(b)), such that; i) ϕ_i is the angle between the plane $\hat{n}_{i-1} - \hat{o}_{i-1}$ and the plane on which the bending occurs,[1] ii) θ_i is the relative rotation between the two reference systems expressed on the latter plane, iii) δL_i is the change in length of the central axis. A $\delta L_i \equiv 0$ identifies a CC segment of constant length, while a $\delta L_i \neq 0$ describes a change of length w.r.t the rest value $L_{0,i} \in \mathbb{R}$. Therefore only δL_i greater than $-L_{0,i}$ are physically meaningful. ϕ_i is also called direction of bending, and θ_i angle of curvature. The resulting inverse mapping for the i-th segment takes the form

$$R^i_{i-1} = \begin{bmatrix} \mathrm{c}^2_{\phi_i}(\mathrm{c}_{\theta_i} - 1) + 1 & \mathrm{s}_{\phi_i}\mathrm{c}_{\phi_i}(\mathrm{c}_{\theta_i} - 1) & \mathrm{c}_{\phi_i}\mathrm{s}_{\theta_i} \\ \mathrm{s}_{\phi_i}\mathrm{c}_{\phi_i}(\mathrm{c}_{\theta_i} - 1) & \mathrm{s}^2_{\phi_i}(\mathrm{c}_{\theta_i} - 1) + 1 & \mathrm{s}_{\phi_i}\mathrm{s}_{\theta_i} \\ -\mathrm{c}_{\phi_i}\mathrm{s}_{\theta_i} & -\mathrm{s}_{\phi_i}\mathrm{s}_{\theta_i} & \mathrm{c}_{\theta_i} \end{bmatrix},$$

$$t^i_{i-1} = \frac{L_{0,i} + \delta L_i}{\theta_i} \begin{bmatrix} \mathrm{c}_{\phi_i}(1 - \mathrm{c}_{\theta_i}) & \mathrm{s}_{\phi_i}(1 - \mathrm{c}_{\theta_i}) & \mathrm{s}_{\theta_i} \end{bmatrix}^{\mathrm{T}}, \tag{2}$$

with c_{ϕ_i}, s_{ϕ_i}, c_{θ_i}, s_{θ_i} being $\cos(\phi_i)$, $\sin(\phi_i)$, $\cos(\theta_i)$, $\sin(\theta_i)$ respectively. $L_{0,i} \in \mathbb{R}$ is the rest length of the central axis of the segment.

In the following we refer to $\alpha_i = [\phi_i\ \ \theta_i\ \ \delta L_i]^{\mathrm{T}} \in \mathbb{R}^3$ as configuration of the i-th segment in the α- parametrization. $\alpha \in \mathbb{R}^{3n}$ is the configuration of the soft robot, which collects α_i for all the segments. It is important to underline that the η_α^{-1} so defined is not a isomorphism. Indeed

$$T^i_{i-1}(\phi_i, 0, \delta L_i) = T^i_{i-1}(\gamma, 0, \delta L_i)\ \ \forall\ \phi_i, \delta L_i, \gamma\ . \tag{3}$$

Therefore, there are infinite choices of the vector α_i describing a single physical configuration; the one in which the robot is straight.

It is worth to stress that T^i_{i-1} refers to both position and orientation.

This condition is graphically illustrated by Fig. 1, where the single red dot in $\mathfrak{M}_i$ - representing the straight segment in Fig. 3(a) - is mapped to a whole line in α_i. Therefore, by looking at the configuration through α_i, one could think that physical motions can be produced by keeping $\theta_i \equiv 0$, and varying ϕ_i. This is however not the case.

[1]The plane created by linear combinations of $\{\hat{n}_i\}_{i-1}$ and $\{\hat{e}_i\}_{i-1}$ is thus the one in which the bending occurs if $\phi_i = 0$.

This flaw is reflected into the Jacobian of the transformation. We consider for simplicity only the translational part of T^i_{i-1}. Its Jacobian can be evaluated by direct differentiation of t^i_{i-1} in (1)

$$ {}^{x}J_{\alpha,i} = \begin{bmatrix} \frac{\mathrm{s}_{\phi_i}\left(\mathrm{c}_{\theta_i}-1\right)L_i}{\theta_i} & \frac{\mathrm{c}_{\phi_i}L_i\left(\mathrm{c}_{\theta_i}+\theta_i\,\mathrm{s}_{\theta_i}-1\right)}{\theta_i^2} & \frac{\mathrm{c}_{\phi_i}\left(1-\mathrm{c}_{\theta_i}\right)}{\theta_i} \\ \frac{\mathrm{c}_{\phi_i}\left(1-\mathrm{c}_{\theta_i}\right)L_i}{\theta_i} & \frac{\mathrm{s}_{\phi_i}L_i\left(\mathrm{c}_{\theta_i}+\theta_i\,\mathrm{s}_{\theta_i}-1\right)}{\theta_i^2} & \frac{\mathrm{s}_{\phi_i}\left(1-\mathrm{c}_{\theta_i}\right)}{\theta_i} \\ 0 & -\frac{L_i\left(\mathrm{s}_{\theta_i}-\theta_i\,\mathrm{c}_{\theta_i}\right)}{\theta_i^2} & \frac{\mathrm{s}_{\theta_i}}{\theta_i} \end{bmatrix}, \quad (4) $$

with $L_i = L_{0,i} + \delta L_i$. The Jacobian determinant is

$$ \det({}^{x}J_{\alpha,i}) = -\frac{\left(\cos\left(\theta_i\right)-1\right)^2\left(\delta L_i + L_{0,i}\right)^2}{\theta_i^3}, \quad (5) $$

which tends to zero for $\theta_i \to 0$. Thus (4) loses rank in the straight configuration. Similar observations can be drawn for the rotational part of T^i_{i-1}. This shortcoming reflects into many aspects of the PCC soft robot's kinematics and dynamics, producing a variety of pathological behaviors that we will discuss in the next sections.

Fig. 3 shows also other two issues affecting the standard α-parametrization. Even outside the straight condition, the two configurations (ϕ_i, θ_i) and $(\phi_i - \pi, -\theta_i)$ describe the same physical posture - as depicted in Panel (b). Panel (c) shows a segment moving in space. This can cause a discontinuity in the evolution expressed in ϕ_i, θ_i if the robot crosses the plane corresponding to the extreme values of ϕ_i.

Finally, the actual chart $\eta_{\alpha,i} : \mathfrak{M}_i \setminus \{N\} \to \mathbb{R}^3$ can be evaluated everywhere outside the straight configuration as [12]

$$ \theta_i = \mathrm{sign}(t^i_{i-1}[3])\,|\arcsin\sqrt{(R^i_{i-1}[1,3])^2 + (R^i_{i-1}[2,3])^2}|, $$

$$ \delta L_i = t^i_{i-1}[3]\frac{\theta_i}{\sin\theta_i} - L_0, \quad \phi_i = \arctan\left(\frac{t^i_{i-1}[2]}{t^i_{i-1}[1]}\right), \quad (6) $$

where $R^i_{i-1}[j,k]$ is the (j,k)-th element of R^i_{i-1}, and $t^i_{i-1}[j]$ is the j-th element of t^i_{i-1} in (1). η_α is then defined as the function collecting all the $\eta_{\alpha,i}$.

III. New Parametrization: A Single Chart Covering the Whole Manifold

In this section, we introduce a new description of the soft robot configuration, defined by an isomorphism η_q between the entire manifold $\mathfrak{M}$ and $\mathbb{R}^{3n}$ (see Fig. 1). In this way we prove that the singularity problem discussed above is not a topological feature of the manifold $\mathfrak{M}_i$ itself. This is reflected in a number of practical advantages, that we discuss in the next sections. This description is derived under the standard PPC hypotheses discussed for the standard parametrization. In the following, we evaluate the isomorphism $\eta_q : \mathfrak{M} \to \mathbb{R}^{3n}$ in two steps. First, we evaluate $\eta_q^{-1} : \mathbb{R}^{3n} \to \mathfrak{M}$ as combination of $\eta_\alpha^{-1} : \mathbb{R}^{3n} \to \mathfrak{M}$ and a function $m : \mathbb{R}^{3n} \to \mathbb{R}^{3n}$ mapping the old configuration into the new one. As a second step, we show that η_q^{-1} is invertible everywhere, and we obtain η_q by inverting it.

A. Arc Lengths

Before introducing the map $m(\cdot)$, we need to discuss some relevant quantities characterizing a CC segment.

We make here the assumption that each arc included in a segment volume has same curvature. We also assume that the bending of all the arcs take place on parallel planes. Consider

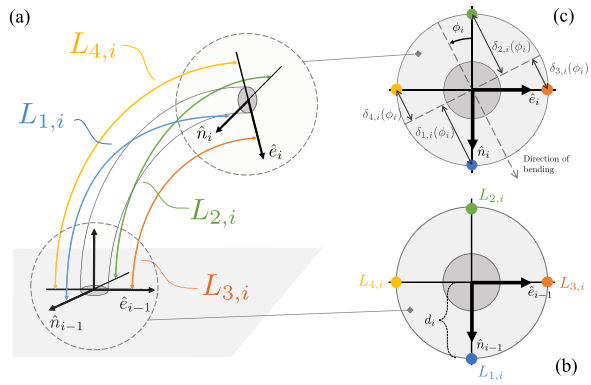

Fig. 4. Representation of the proposed q-parametrization, for the i-th segment of a PCC robot. The left part of the figure - Panel (a) - shows the i-th CC segment of a soft robot. The parameters q_i are defined as a linear combination of the lengths of the four arcs highlighted in figure. The two ends of each arc are connected at a distance d_i from the origin of $\{S_{i-1}\}$ and $\{S_i\}$. These connections are shown by the the right side of this figure - Panels (b) and (c) respectively - which presents the cross sections of the two ends of the CC segment. Relevant quantities are underlined in figure.

now the four arcs highlighted in Fig. 4. They have one of their ends connected to the frame $\{S_{i-1}\}$, as show by the left side of the figure. The other end is connected to the frame $\{S_i\}$, as shown by the right side of the figure. More specifically the first arc has one end connected to $[d_i, 0, 0]^{\mathrm{T}}$ expressed in $\{S_{i-1}\}$, and the other to $[d_i, 0, 0]^{\mathrm{T}}$ expressed in $\{S_i\}$. Similarly the other three arcs are connected to $[-d_i, 0, 0]^{\mathrm{T}}$, $[0, d_i, 0]^{\mathrm{T}}$, and $[0, -d_i, 0]^{\mathrm{T}}$.

We call $\delta_{j,i}$ the distance between the end of the j-th arc on the top side, and the straight line included in the plane $\hat{n}_i$-$\hat{e}_i$, perpendicular to the direction of bending, and passing through the central axis of the segment - as shown by right side of Fig. 4. Trigonometric considerations yield the following expressions for these distances

$$ \begin{aligned} \delta_{1,i}(\phi_i) &= +d_i\cos(\phi_i), \quad & \delta_{2,i}(\phi_i) &= -d_i\cos(\phi_i), \\ \delta_{3,i}(\phi_i) &= +d_i\sin(\phi_i), \quad & \delta_{4,i}(\phi_i) &= -d_i\sin(\phi_i)\ , \end{aligned} \quad (7) $$

where ϕ_i is the direction of bending, as defined in Section II.

Consider now the plane on which the j-th arc bends. The cross-section that it identifies is shown in Fig. 2(c). The length of the four arcs can thus be evaluated through simple geometric considerations as $L_{\delta_{j,i}} = \theta_i(\frac{L_i}{\theta_i} - \delta_{j,i}) = L_i - \theta_i\delta_{j,i}$, where $L_i = L_{0,i} + \delta L_i$ is the length of the central axis of the segment, and θ_i is the the angle of curvature as defined in Section II. Combining this equation with (7) leads to the closed form of the four lengths as function of α_i

$$ \begin{aligned} L_{1,i}(\phi_i, \theta_i, \delta L_i) &= L_{0,i} + \delta L_i - \theta d_i\cos(\phi_i), \\ L_{2,i}(\phi_i, \theta_i, \delta L_i) &= L_{0,i} + \delta L_i + \theta d_i\cos(\phi_i), \\ L_{3,i}(\phi_i, \theta_i, \delta L_i) &= L_{0,i} + \delta L_i - \theta d_i\sin(\phi_i), \\ L_{4,i}(\phi_i, \theta_i, \delta L_i) &= L_{0,i} + \delta L_i + \theta d_i\sin(\phi_i). \end{aligned} \quad (8) $$

B. Improved Parametrization

We calculate the difference in length between the two arcs having one of their ends connected along $\hat{n}_{i-1}$, and between the

remaining two

$$\Delta_{\mathrm{x},i} = \frac{L_{2,i} - L_{1,i}}{2} = \theta_i d_i \cos(\phi_i),$$
$$\Delta_{\mathrm{y},i} = \frac{L_{4,i} - L_{3,i}}{2} = \theta_i d_i \sin(\phi_i). \tag{9}$$

These two variables contain all the information about θ_i and ϕ_i, and at the same time they have a direct connection to physical quantities. Even more importantly, (9) is such that all the α_i such that $\theta_i = 0$ - i.e. in the straight configuration - are mapped to a single value regardless the value of ϕ_i. In this way all the redundant representations collapse into a single non redundant one (see Fig. 1).

We therefore propose to use $\Delta_{\mathrm{x},i}$ and $\Delta_{\mathrm{y},i}$ as a substitute for θ_i and ϕ_i, yielding the transition map

$$\begin{bmatrix} \phi \\ \theta \\ \delta L \end{bmatrix} \xrightarrow{m(\cdot)} \begin{bmatrix} \Delta_{\mathrm{x}} \\ \Delta_{\mathrm{y}} \\ \delta L \end{bmatrix}. \tag{10}$$

We will call in the following $q_i = \begin{bmatrix} \Delta_{\mathrm{x},i} & \Delta_{\mathrm{y},i} & \delta L_i \end{bmatrix}^{\mathrm{T}} \in \mathbb{R}^3$ configuration of the i-th segment in the new parametrization, $q \in \mathbb{R}^{3n}$ is the vector collecting all the q_i, and it is the configuration vector of the robot expressed in the new parametrization.

The explicit expression for $m_i(\cdot)$ is

$$\phi_i(q_i) = \arccos\left(\frac{\Delta_{\mathrm{x},i}}{\Delta_i}\right) = \arcsin\left(\frac{\Delta_{\mathrm{y},i}}{\Delta_i}\right),\ \theta_i(q_i) = \frac{\Delta_i}{d_i}, \tag{11}$$

f The Jacobian ${}^{\alpha}J_q$ of $m(q)$ is block diagonal, and the i-th block can be obtained by direct derivation of (11)

$${}^{\alpha}J_{q,i}(q_i) = \frac{1}{d_i \Delta_i^2} \begin{bmatrix} -d_i\Delta_{\mathrm{y},i} & d_i\Delta_{\mathrm{x},i} & 0 \\ \Delta_i\Delta_{\mathrm{x},i} & \Delta_i\Delta_{\mathrm{y},i} & 0 \\ 0 & 0 & d_i\Delta_i^2 \end{bmatrix}. \tag{12}$$

C. Inverse Chart

We evaluate the inverse chart $\eta_{\mathrm{q}}^{-1} : \mathfrak{M} \to \mathrm{R}^{3n}$ by composition

$$\eta_{\mathrm{q}}^{-1} = m^{-1} \circ \eta_{\alpha}^{-1}, \tag{13}$$

where η_{α}^{-1} and m^{-1} are defined in (2) and (11). Simple algebraic steps lead to the explicit form (14) shown at the bottom of this page, where $\Delta_i = \sqrt{\Delta_{\mathrm{x},i}^2 + \Delta_{\mathrm{y},i}^2}$.

To assure that η_{q}^{-1} is actually the inverse of a function η_{q} - i.e. that it is invertible - we evaluate its Jacobian. Combining (12) and (4) yields

$${}^{x}J_q(\Delta_{\mathrm{x}}, \Delta_{\mathrm{y}}, \delta L) = {}^{x}J_{\alpha}(m(q))\ {}^{\alpha}J_q(q)\ . \tag{15}$$

We can not report its explicit form for the sake of space. We report instead its determinant, with $\Delta_i = \sqrt{\Delta_{\mathrm{x},i}^2 + \Delta_{\mathrm{y},i}^2}$,

$$\det({}^{x}J_q) = \left(\cos\left(\frac{\Delta_i}{d_i}\right) - 1\right)^2 \frac{(\delta L_i + L_{0,i})^2}{(\Delta_i/d_i)^4}, \tag{16}$$

which is strictly positive and with limits in $\Delta_i \to 0$ (straight configuration) well defined, and equal to $(\delta L_i + L_{0,i})^2/4$. Evaluating the Jacobian for the rotational part would lead to similar results, that we will report in future work.

Thus, η_q exists and it is an isomorphism by construction.

D. Atlas

We build now η_{q} by inverting the η_{q}^{-1} just derived. The values of q_i can be calculated by inspection, yielding

$$\Delta_{\mathrm{x},i} = t_{i-1}^i[1]\,\Delta_{\mathrm{c}}(\delta L), \quad \Delta_{\mathrm{y},i} = t_{i-1}^i[2]\,\Delta_{\mathrm{c}}(\delta L),$$
$$\delta L_i = t_{i-1}^i[3] \frac{d_i\ \arccos(R_{i-1}^i[3,3])}{\sin(\arccos(R_{i-1}^i[3,3]))} - L_{0,i}, \tag{17}$$

where $R_{i-1}^i[j,k]$ and $t_{i-1}^i[j]$ are defined as above, and

$$\Delta_{\mathrm{c}}(\delta L) = \frac{d_i}{L_0 + \delta L} \frac{\arccos(R_{i-1}^i[3,3])^2}{R_{i-1}^i[3,3] - 1}\ .$$

For the sake of space and readability, we consider $d_i = 1$m in the rest of the letter. Note that this is a free parameter, that we could also choose to match some specific location, e.g. where strain sensors are placed, so to have direct readings of the configuration.

IV. Dynamics

As discussed in [5], [12], PCC soft robots are Lagrangian systems and their dynamics can be expressed in the standard form. For the classic α-parametrization the following results

$$B_{\alpha}(\alpha)\ddot{\alpha} + C_{\alpha}(\alpha, \dot{\alpha})\dot{\alpha} + K_{\alpha}\alpha + D_{\alpha}(\alpha)\dot{\alpha} = A_{\alpha}(\alpha)\, u, \tag{18}$$

where $\alpha \in \mathbb{R}^{3n}$ is the configuration vector as introduced in Section II, with its time derivatives $\dot{\alpha}, \ddot{\alpha} \in \mathbb{R}^{3n}$. $B_{\alpha} \in \mathbb{R}^{3n \times 3n}$ is the inertia matrix, $C_{\alpha}\dot{\alpha} \in \mathbb{R}^{3n}$ collects Coriolis and centrifugal forces, $K_{\alpha}\alpha \in \mathbb{R}^{3n}$ is the linear elastic field, and $D_{\alpha}(\alpha)\dot{\alpha} \in \mathbb{R}^{3n}$ is the configuration dependent damping. $A_{\alpha} \in \mathbb{R}^{3n \times 3n}$ maps the input $u \in \mathbb{R}^{3n}$ in wrenches producing independent accelerations $\ddot{\alpha}$. Eq. (18) is a standard ordinary differential equation if B_{α} is full rank, and it is completely actuated if A_{α} is full rank. We will show in the following that neither of these two conditions can be fulfilled everywhere, when using the α-parametrization.

$$R_{i-1}^i = \begin{bmatrix} 1 + \frac{\Delta_{\mathrm{x},i}^2}{\Delta_i^2}\left(\cos\left(\frac{\Delta_i}{d_i}\right) - 1\right) & \frac{\Delta_{\mathrm{x},i}\Delta_{\mathrm{y},i}}{\Delta_i^2}\left(\cos\left(\frac{\Delta_i}{d_i}\right) - 1\right) & \frac{-\Delta_{\mathrm{x},i}}{\Delta_i}\sin\left(\frac{\Delta_i}{d_i}\right) \\ \frac{\Delta_{\mathrm{x},i}\Delta_{\mathrm{y},i}}{\Delta_i^2}\left(\cos\left(\frac{\Delta_i}{d_i}\right) - 1\right) & 1 + \frac{\Delta_{\mathrm{y},i}^2}{\Delta_i^2}\left(\cos\left(\frac{\Delta_i}{d_i}\right) - 1\right) & \frac{-\Delta_{\mathrm{y},i}}{\Delta_i}\sin\left(\frac{\Delta_i}{d_i}\right) \\ \frac{\Delta_{\mathrm{x},i}}{\Delta_i}\sin\left(\frac{\Delta_i}{d_i}\right) & \frac{\Delta_{\mathrm{y},i}}{\Delta_i}\sin\left(\frac{\Delta_i}{d_i}\right) & \cos\left(\frac{\Delta_i}{d_i}\right) \end{bmatrix}$$
$$t_{i-1}^i = \frac{d_i(L_{0,i} + \delta L_i)}{\Delta_i^2} \begin{bmatrix} \Delta_{\mathrm{x},i}\left(1 - \cos\left(\frac{\Delta_i}{d_i}\right)\right) \\ \Delta_{\mathrm{y},i}\left(1 - \cos\left(\frac{\Delta_i}{d_i}\right)\right) \\ \Delta_i\ \sin\left(\frac{\Delta_i}{d_i}\right) \end{bmatrix} \tag{14}$$

Similarly, using the here proposed parametrization yields the following dynamics

$$B(q)\ddot{q} + C(q,\dot{q})\dot{q} + Kq + D\dot{q} = A(q)\,u \tag{19}$$

with symbols defined in analogy to (18).

We derive in the next subsections the terms of both (18) and (19), underling the flows of the first, and how they are overcame in the second.

A. Singularity of the Inertia Matrix

A first main issue generated by the α-description of the state is the inertia matrix that it produces. Consider as an example the simple case of single point mass μ, connected at the tip of a CC segment. The inertia matrix can be evaluated as follows by using the Jacobian (4)

$$B_\alpha = \mu \left({}^{x}J_\alpha^{\mathrm{T}}\,{}^{x}J_\alpha\right) = \mu \begin{bmatrix} b_{\phi\phi}(\theta,\delta L) & 0 & 0 \\ 0 & * & * \\ 0 & * & * \end{bmatrix}, \tag{20}$$

where the asterisks are non null elements that we do not report for the sake of space, and

$$b_{\phi\phi}(\theta,\delta L) = \frac{(\cos(\theta)-1)^2}{\theta^2}(\delta L + L_0)^2\,, \tag{21}$$

which is the rotational inertia associated to $\ddot{\phi}$. As anticipated, $\lim_{\theta\to 0} b_{\phi\phi}(\theta,\delta L) = 0$. Thus B_α loses rank in the straight configuration, making (18) a differential algebraic equation, which is of course much more difficult to study, control, and simulate [19] than a standard ordinary differential equation. We will discuss the effect of this shortcoming in the simulations reported in following sections. Note that this behavior can not be prevented even adding rotational inertia. Indeed, the issue is produced by the fact that when $\theta = 0$ the robot does not physically move when ϕ changes.

We evaluate now the inertia matrix in q-space, using (15)

$$\begin{aligned} B &= \mu \left({}^{x}J_q^{\mathrm{T}}\,{}^{x}J_q\right) \\ &= \mu \begin{bmatrix} b_{\mathrm{xx}} & \frac{\Delta_\mathrm{x}\Delta_\mathrm{y} L^2 (\Delta - \mathrm{s}_\Delta)^2}{\Delta^6} & \frac{\Delta_\mathrm{x} D}{\Delta^4} \\ \frac{\Delta_\mathrm{x}\Delta_\mathrm{y} L^2 (\Delta - \mathrm{s}_\Delta)^2}{\Delta^6} & b_{\mathrm{yy}} & \frac{\Delta_\mathrm{y} D}{\Delta^4} \\ \frac{\Delta_\mathrm{x} D}{\Delta^4} & \frac{\Delta_\mathrm{y} D}{\Delta^4} & -\frac{2\,\mathrm{c}_\Delta - 2}{\Delta^2} \end{bmatrix} \end{aligned} \tag{22}$$

where with $D = L\,(2\,\mathrm{c}_\Delta + \mathrm{s}_\Delta\,\Delta - 2)$, $L = \delta L + L_0$, $\Delta = \sqrt{\Delta_\mathrm{x}^2 + \Delta_\mathrm{y}^2}$, $\mathrm{c}_\Delta = \cos(\Delta)$, and $\mathrm{s}_\Delta = \sin(\Delta)$. We do not report b_{xx} and b_{yy} for the sake of space. The limit for $\Delta \to 0$ (straight configuration) is well defined, and it is

$$\lim_{\substack{\Delta_\mathrm{x}\to 0 \\ \Delta_\mathrm{y}\to 0}} B(\Delta_\mathrm{x},\Delta_\mathrm{y},\delta L) = \mu \begin{bmatrix} \frac{(\delta L + L_0)^2}{4} & 0 & 0 \\ 0 & \frac{(\delta L + L_0)^2}{4} & 0 \\ 0 & 0 & 1 \end{bmatrix}, \tag{23}$$

which is full rank for all physically meaningful configurations.[2]

We do not report neither $C_\alpha(q,\dot{q})$ nor $C(q,\dot{q})$ for the sake of space and readability. They share the same characteristics of the respective inertia matrices in terms of well possessedness around the straight configuration.

B. Linear Impedance

As discussed in [12], the elastic field expressed in α space is in the linear form $K\alpha$. The stiffness matrix K_α is block diagonal,

[2]In $\delta L = -L_0$ both (22) and (20) lose rank since the soft robot is so compressed to collapse in a single point.

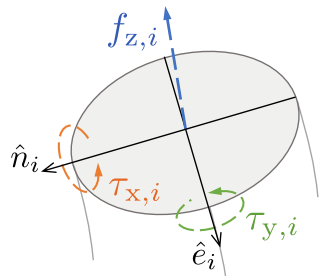

Fig. 5. We consider as control input u_i for the i-th segment, the wrench having as first two elements the torques around $\hat{n}_i$ and $\hat{e}_i$ - called $\tau_{\mathrm{x},i}$ and $\tau_{\mathrm{y},i}$ respectively - and as third the force in the direction of $\hat{o}_i$ - called $f_{\mathrm{z},i}$. Note that - being the wrench internal - the same torques and force are produced with opposite side around the frame $\{S_{i-1}\}$ (not shown in picture).

with i-th block

$$K_{\alpha,i} = \begin{bmatrix} 0 & 0 & 0 \\ 0 & \kappa_{\theta,i} & 0 \\ 0 & 0 & \kappa_{\delta L,i} \end{bmatrix}. \tag{24}$$

To map the elastic force to the new configuration space, we express α_i in terms of q_i through (11), and we map the force produced back to q-space through pre-multiplication for ${}^{\alpha}J_{q,i}$ in (12)- i.e. by using the kineto-static duality [20]. This yields

$${}^{\alpha}J_{q,i}^{\mathrm{T}}(q) K_{\alpha,i}\, m_i(q_i) = \begin{bmatrix} \kappa_{\theta,i} & 0 & 0 \\ 0 & \kappa_{\theta,i} & 0 \\ 0 & 0 & \kappa_{\delta L,i} \end{bmatrix} \begin{bmatrix} \Delta_{\mathrm{x},i} \\ \Delta_{\mathrm{y},i} \\ \delta L_i \end{bmatrix} \doteq K_i q\,, \tag{25}$$

which in addition to being linear is also with full rank stiffness. K is the block diagonal matrix having K_i as i-th block.

The damping acting in α space [12] is $D_\alpha(\theta)\dot{\alpha}$. The matrix $D_\alpha(\theta)$ is block-diagonal, with i-th block

$$D_{\alpha,i}(\theta_i) = \begin{bmatrix} \beta_{\theta,i}\theta_i^2 & 0 & 0 \\ 0 & \beta_{\theta,i} & 0 \\ 0 & 0 & \beta_{\delta L,i} \end{bmatrix}, \tag{26}$$

which is nonlinear, configuration dependent, and it loses rank in $\theta_i = 0$. As for $K\alpha$, the damping expressed in α can be mapped in q through pre-multiplication for ${}^{\alpha}J_q^{\mathrm{T}}$. Furthermore, $\dot{\alpha}$ can be evaluated from $\dot{q}$ through pre-multiplication for the same Jacobian. Therefore, the damping force expressed in q space is $D\dot{q}$. Again, D is block-diagonal, with i-th block

$$D_i \doteq {}^{\alpha}J_{q,i}^{\mathrm{T}}(q) D_{\alpha,i}(m_i(q_i))\,{}^{\alpha}J_{q,i}(q_i) = \begin{bmatrix} \beta_{\theta,i} & 0 & 0 \\ 0 & \beta_{\theta,i} & 0 \\ 0 & 0 & \beta_{\delta L,i} \end{bmatrix}, \tag{27}$$

which, as K_i, is constant and full rank.

C. Singularity of the Input Mapping

As already highlighted by (18) and (19), in soft robots it is usually not possible to exert wrenches acting directly and independently on the accelerations. Instead, the input u is mapped to the state through a configuration dependent transmission matrix, that is different for the two parametrizations. In order for the systems to be fully actuated, these matrices should be full rank. This property is a function of how fine is the discretization of the continuum dynamics of the soft robot. In this work we take a single CC segment for each actuated segment, leading to a square transmission matrix. Even under this coarse discretization, A_α

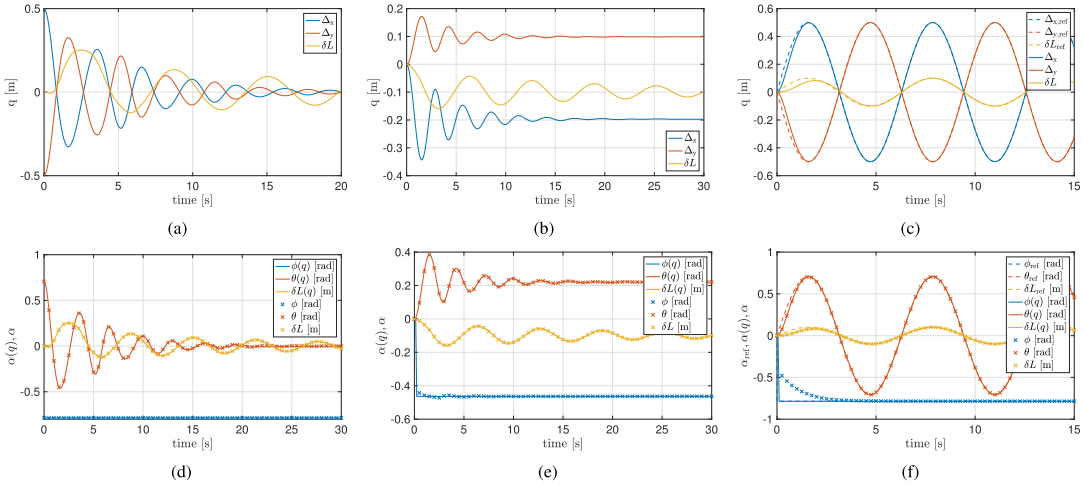

Fig. 6. Results of simulations expressed in the q (panels (a–c)) and α (panels (d-f)) parametrization for a single CC segment, with mass concentrated in its tip. Panels (a,d) show an example of open loop unforced evolutions. Panel (a) shows the evolution when the system is simulated in q-space. Panel (d) shows the evolution simulated in α-space with superimposed $m(q)$, i.e. the estimation of α from the simulation in q. The initial conditions are $q = [0.5\ 0.5\ 0]^{\mathrm{T}}$m, $\dot{q} = [0\ 0\ 0]^{\mathrm{T}}$, $\alpha = m(q)$, $\dot{\alpha} = [0\ 0\ 0]^{\mathrm{T}}$. Panels (b, e) show an example of open loop forced evolutions, with constant input $u \equiv [0.1\ \mathrm{Nm}\ 0.2\ \mathrm{Nm} - 0.1\mathrm{N}]^{\mathrm{T}}$. Panel (b) shows the evolution when the system is simulated in q-space. Panel (e) shows the evolution simulated in α-space with superimposed $m(q)$. The system starts from the equilibrium state $q = 0$, $\alpha = 0$. Panels (c, f) show an example of trajectory tracking in state space, resulting from the application of controllers (35) and (36). The two trajectories α_{ref} and q_{ref} are chosen so to produce the same motion in the robot. Panel (c) shows the resulting evolution in q space, i.e. when using (36). Panel (f) depicts the evolutions in α space obtained using (35), and as $m(q)$.

is not full rank, while A is. We consider here the input vector $u \in R^{3n}$, such that $u_{3i-2} = \tau_{\mathrm{x},i}$, $u_{3i-1} = \tau_{\mathrm{y},i}$, $u_{3i} = f_{\mathrm{z},i}$, as defined in Fig. 5.

We start from the input mapping for α, which is a block diagonal matrix with i-th block defined as

$$A_{\alpha,i}(\alpha) = J_i^{\mathrm{T}}(q) R_0^i(q) - J_{i-1}^{\mathrm{T}}(q) R_0^{i-1}(q), \tag{28}$$

where J_i is the Jacobian matrix mapping $\dot{\alpha}_i$ into the angular velocity expressed around $\hat{n}_i$ and $\hat{e}_i$, and the linear velocity projected on the $\hat{o}_i$. R_0^i is the rotation matrix mapping $\{S_i\}$ into $\{S_0\}$. This latter rotation has the role of making the definition of the wrench local, while the second term in the subtraction takes into account the internal nature of the actuation. Evaluating (28) leads to

$$A_{\alpha,i}(\phi_i, \theta_i, \delta L_i) = \begin{bmatrix} -c_{\phi_i}\, s_{\theta_i} & -s_{\phi_i}\, s_{\theta_i} & 0 \\ -s_{\phi_i} & c_{\phi_i} & (L_{0,i} + \delta L_i)\, \dfrac{\theta_i - s_{\theta_i}}{{\theta_i}^2} \\ 0 & 0 & \dfrac{s_{\theta_i}}{\theta_i} \end{bmatrix}. \tag{29}$$

where c_{ϕ_i}, s_{ϕ_i}, c_{θ_i}, s_{θ_i} are $\cos(\phi_i)$, $\sin(\phi_i)$, $\cos(\theta_i)$, $\sin(\theta_i)$ respectively, and $L_{0,i}$ is the rest length of the central axis of the segment. In the straight configuration the matrix is

$$A_{\alpha,i}(\phi_i, 0, \delta L_i) = \begin{bmatrix} 0 & 0 & 0 \\ -s_{\phi_i} & c_{\phi_i} & 0 \\ 0 & 0 & 1 \end{bmatrix}, \tag{30}$$

which is not full rank and thus not invertible. This is a strong limitation for the development of feedback controllers, since it prevents the introduction of the full actuation hypothesis around the straight configuration.

Also this problem is solved by the proposed parametrization. Matrix A in (19) can be evaluated by using the kineto-static duality; we map a torque expressed in α to a torque expressed in q by pre-multiplication of the Jacobian in (12). The following matrix results

$$A(q) = {}^{\alpha}J_q^{\mathrm{T}}(\Delta_{\mathrm{x}}, \Delta_{\mathrm{y}}, \delta L) A_{\alpha}(m(\Delta_{\mathrm{x}}, \Delta_{\mathrm{y}}, \delta L)), \tag{31}$$

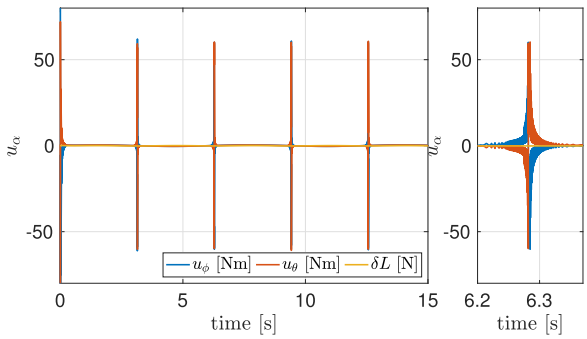

Fig. 7. Control action exerted by (35) during trajectory tracking of a sinusoidal reference trajectory. Each time the system gets close to the condition $\theta \simeq 0$, A_α becomes bad conditioned, and the control action increases consequently. The right side reports one of the spikes zoomed to reveal high frequency chattering.

which is again block diagonal, with diagonal elements $A_i(q_i)$ equal to

$$\begin{bmatrix} \dfrac{\Delta_{\mathrm{x},i}\, \Delta_{\mathrm{y},i}\, D_i}{\Delta_i^3} & \dfrac{-\Delta_{\mathrm{x},i}^2\, \Delta_i - \Delta_{\mathrm{y},i}^2 \sin(\Delta_i)}{\Delta_i^3} & \dfrac{\Delta_{\mathrm{x},i}\, D_i\, L_i}{\Delta_i^3} \\ \dfrac{\Delta_{\mathrm{y},i}^2\, \Delta_i + \Delta_{\mathrm{x},i}^2 \sin(\Delta_i)}{\Delta_i^3} & \dfrac{-\Delta_{\mathrm{x},i}\, \Delta_{\mathrm{y},i}\, D_i}{\Delta_i^3} & \dfrac{\Delta_{\mathrm{y},i}\, D_i\, L_i}{\Delta_i^3} \\ 0 & 0 & \dfrac{\sin(\Delta_i)}{\Delta_i} \end{bmatrix}, \tag{32}$$

with $\Delta_i = \sqrt{\Delta_{\mathrm{x},i}^2 + \Delta_{\mathrm{y},i}^2}$, $L_i = \delta L_i + L_{0,i}$, and $D_i = \Delta_i - \sin(\Delta_i)$. The limit in the straight configuration is well defined and full rank. Thus system (18) is not completely actuated everywhere, while (19) is.

D. Simulations

The above discussed terms can be used to simulate the system in α-parametrization as $\ddot{\alpha} = -B_\alpha^{\mathrm{I}}(\alpha)(C_\alpha(\alpha, \dot{\alpha})\dot{\alpha} + K_\alpha \alpha + D_\alpha(\alpha)\dot{\alpha} - A_\alpha(\alpha)\, u)$, where we heuristically defined a

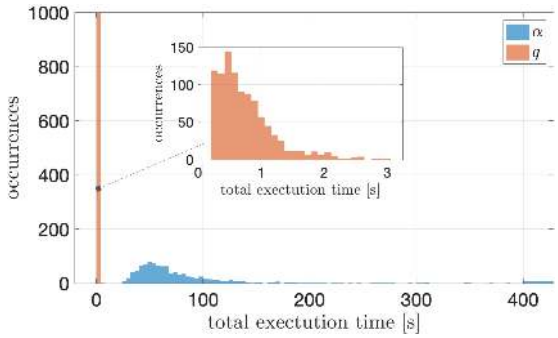

Fig. 8. The evaluation of the closed loop expressed in α is substantially more onerous than the one expressed in q. This histogram is produced by collecting execution times from the trajectory tracking of 10^3 sinusoids with random amplitude and frequency, each one simulated for 15 seconds.

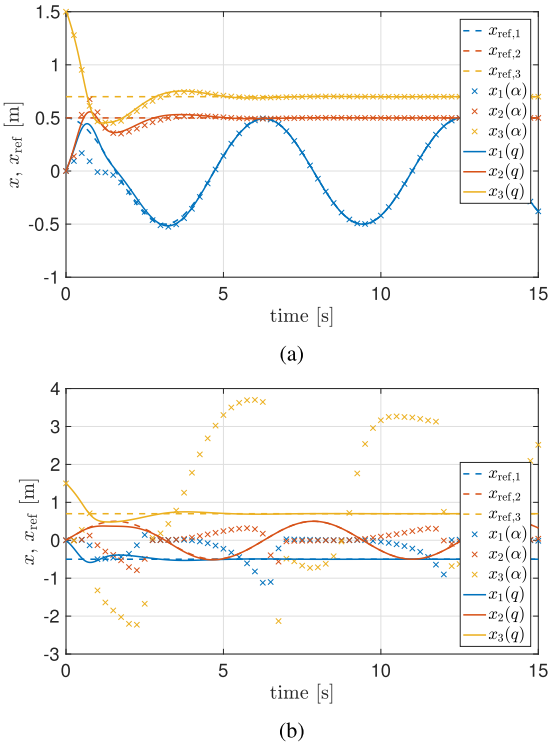

Fig. 9. Tracking of a trajectory in Cartesian space with the robot's tip. In panel (a) the evolution does not reach configurations near to $\phi \simeq \pm\pi$, and it passes only one time from the straight configuration. Thus the controller designed in α space (crosses in figure) only has a 1 second delay in reaching the reference (dashed line) if compared with the one designed in q space (solid line). In panel (b) instead the robot is asked to cross that boundary several time, resulting in a completely inconsistent behavior when the controller designed in α is used. Very good performance are instead obtained with the controller designed in q space.

continuation for the inverse of B_α as $B_\alpha^{\mathrm{I}}(\alpha) = B_\alpha^{-1}(r(\alpha))$; $r(\cdot)$ substitutes to each θ_i a value ϵ, if $|\theta_i| < \epsilon$. In the following we consider $\epsilon = 10^{-2}$. Since all the terms in (19) are well defined, we can directly integrate the dynamics in the usual way $\ddot{q} = -B^{-1}(q)(C(q,\dot{q})\dot{q} + Kq + D\dot{q} - A(q)\,u)$.

We consider here a single constant curvature segment, with a 1 Kg mass concentrated in its tip and negligible inertia (see Section IV-A). The other parameters are $\kappa_\theta = 1\frac{\mathrm{Nm}}{\mathrm{rad}}, \kappa_{\delta L} = 1\frac{\mathrm{N}}{\mathrm{m}}, L_0 = 1\mathrm{m}, \beta_\theta = 0.1\frac{\mathrm{Nms}}{\mathrm{rad}}, \beta_{\delta L} = 0.1\frac{\mathrm{Ns}}{\mathrm{m}}$. Fig. 6(a) and 6(d) show the results of a simulation with $u \equiv 0$, and with the initial conditions $q(0) = [0.5\ 0.5\ 0]^{\mathrm{T}}\mathrm{m}$, $\dot{q}(0) = [0\ 0\ 0]^{\mathrm{T}}$, $\alpha(0) = m(q(0))$, $\dot{\alpha}(0) = [0\ 0\ 0]^{\mathrm{T}}$. We evaluate ϕ and θ from q, and we plot them together with the ones obtained by directly integrating $\ddot{\alpha}$ in Fig. 6(d). The two evolutions are perfectly superimposed. Fig. 6(b) and 6(e) show a step response for the same soft robot, starting from rest conditions. The amplitude of the step is $[0.1\ \mathrm{Nm}\ 0.2\ \mathrm{Nm} - 0.1\ \mathrm{N}]^{\mathrm{T}}$. Again, the two evolutions are superimposed. These simulations further confirm that the q-parametrization is a proper alternative to α one. We will show through simulations the advantages of the first w.r.t. the latter in Section V-B.

V. Closed Loop

In this section we consider the limitations of the classic parametrization - and how the proposed one solves them - for what concerns the closure of the loop.

A. Controller

We specify the trajectory in state space implementing a desired evolution of the robot's tip in Cartesian space x_{ref}, through a standard Jacobian based kinematic inversion algorithm

$$\dot{\alpha}_{\mathrm{ref}} = {}^{x}J_\alpha{}^{+}(\dot{x}_{\mathrm{d}} + k_{\mathrm{x}}(x_{\mathrm{d}} - x)), \tag{33}$$

and

$$\dot{q}_{\mathrm{ref}} = {}^{x}J_q{}^{+}(\dot{x}_{\mathrm{d}} + k_{\mathrm{x}}(x_{\mathrm{d}} - x)), \tag{34}$$

where $x \in \mathbb{R}^3$ is the position of the robot's tip in Cartesian coordinates. The control action regulating the system on α_{ref} and q_{ref} is the one proposed in [5]

$$\begin{aligned} u = A_\alpha^{\mathrm{I}}(\alpha)(&-B_\alpha(\alpha)\ddot{\alpha}_{\mathrm{ref}} - C_\alpha(\alpha,\dot{\alpha})\dot{\alpha}_{\mathrm{ref}} - K_\alpha\alpha_{\mathrm{ref}} \\ &- D_\alpha(\alpha)\dot{\alpha}_{\mathrm{ref}} + K_{\mathrm{P}}(\alpha_{\mathrm{ref}} - \alpha) - K_{\mathrm{D}}(\dot{\alpha}_{\mathrm{ref}} - \dot{\alpha})), \end{aligned} \tag{35}$$

and

$$\begin{aligned} u = A^{-1}(q)(&-B(q)\ddot{q}_{\mathrm{ref}} - C(q,\dot{q})\dot{q}_{\mathrm{ref}} - Kq_{\mathrm{ref}} \\ &- D\dot{q}_{\mathrm{ref}} + K_{\mathrm{P}}(q_{\mathrm{ref}} - q) - K_{\mathrm{D}}(\dot{q}_{\mathrm{ref}} - \dot{q})). \end{aligned} \tag{36}$$

It is important to underline that, while the structure of the two controllers is the same, the resulting algorithms are deeply different due to the parametrization.

B. Simulations

We consider $\kappa_{\mathrm{x}} = 100$, $K_{\mathrm{P}} = 1$, $K_{\mathrm{D}} = 1$. The dynamical systems are the same used in Section IV-D, i.e. single CC segment with mass concentrated in its tip. We first test the performances of the two controllers (35) and (36) in tracking a trajectory in configuration space. The two references are selected so to map in a same trajectory in $\mathfrak{M}$, i.e. $q_{\mathrm{ref}} = [0.5,\ -0.5,\ 0.1]\sin(t)\mathrm{m}$, and $\alpha_{\mathrm{ref}} = m^{-1}(q_{\mathrm{ref}})$. The derivatives are evaluated accordingly. Note that α_{ref} is cosinusoidal too. The initial condition is the straight configuration. Fig. 6(c) and 6(f) report the results of this simulation. The system controlled by (36) reaches the steady state in about 1s, while the one controlled by (35) takes about 4s. Panel (b) of the same figure shows that this slower behavior is to be inputed to the discussed issues in ϕ.

While this is not a desirable behavior, it is not the main issue of (35). Fig. 7 shows the control action generated during the tracking of the trajectory just discussed. Each time the system gets close to the singularity, the control action starts to chatter and it spikes up to 50 times the maximum torque it would produce otherwise. Neither the spikes nor the chattering are present when using (36).

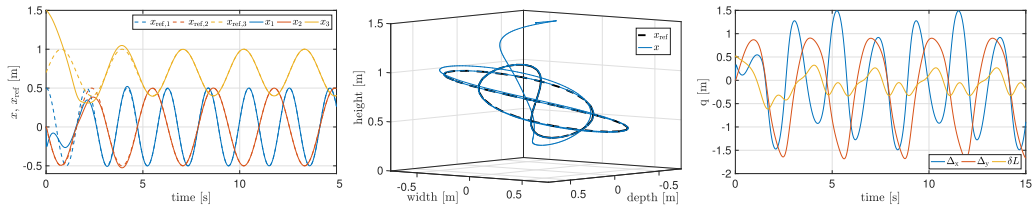

(a) (b) (c)

Fig. 10. A soft CC segment is controlled through (36) and (34), to follow a Lissajous curve with its tip. This behavior can not be produced by using a controller designed in α, since it involves having ϕ crossings of the $\pm\pi$ boundary, and the robot moving close the straight configuration. Panel (a) shows the evolution of the tip position in time. Panel (b) depicts the evolution of the tip in Cartesian space. Panel (c) reports the evolution in time of q.

Another pathological behavior of (35) can be spotted by looking at execution times. To test the efficiency of the two algorithms in terms of computational resources needed, the two models are simulated on a same computer and in same conditions. Fig. 8 reports an histogram collecting the execution times of one thousand trajectory tracking simulations, with $q_{\text{ref}} = -[1; 1; 0.25]\text{m} + [\hat{\phi},\ \hat{\theta},\ \hat{\delta L}]\ \sin(\omega t)$, with $\hat{\phi}$, $\hat{\theta}$, $\hat{\delta L}$ and ω extracted from an uniform distribution ranging from 0 to 2 m, 2 m, 0.25 m, 10 Hz respectively, and $\alpha_{\text{ref}} = m^{-1}(q_{\text{ref}})$. We used `MatLab2017b`. No extra task was executed on the computer during the simulations. Dormand-Price variable step algorithm was used for integration, with minimum sampling rate 10Hz and relative tolerance 10^{-4}. Larger values of relative tolerance generate instable behaviors when α parametrization is used. The closed loop (35) is $\sim$10 times more computationally onerous to evaluate than (36).

We now close the loop with the kinematic inversion algorithms (33) and (34). Fig. 9(a) shows the tracking of a sinusoidal trajectory in Cartesian space. Both control architectures work with comparable results. When instead the robot is asked to cross the boundary of $\phi = \pm\pi$, the differences between the two controllers become dramatic, as illustrated by Fig. 9(b). Finally, Fig. 10 shows the tracking of a more complex trajectory in Cartesian space. Only the controller built with the here proposed q-parametrization - i.e. (36) and (34) - is able to perform the task. We did not report the performance of the system controlled with (35) and (33), since it diverged very rapidly.

VI. Conclusions and Future Work

This work analyzed an improved parametrization for the state space of three dimensional soft robots with piecewise constant curvature. It then discussed the main limitations of the standard PCC parametrization, and it showed that the new one solves them. The main focus of the work has been on the control application of the considered parametrization. Future work will be devoted to testing the use of the proposed parametrization with experiments on a real robot. We will also investigate the use of this parametrization in combination with polynomial curvature models [21], to extend the latter to the 3D case.

Acknowledgment

The authors would like to thank NSF for this support.

References

[1] T. G. Thuruthel, Y. Ansari, E. Falotico, and C. Laschi, "Control strategies for soft robotic manipulators: A survey," *Soft Robot.*, vol. 5, no. 2, pp. 149–163, 2018.

[2] D. Rus and M. T. Tolley, "Design, fabrication and control of soft robots," *Nature*, vol. 521, no. 7553, pp. 467–475, 2015.

[3] T. G. Thuruthel, E. Falotico, M. Manti, and C. Laschi, "Stable open loop control of soft robotic manipulators," *IEEE Robot. Autom. Lett.*, vol. 3, no. 2, pp. 1292–1298, Apr. 2018.

[4] M. Thieffry, A. Kruszewski, O. Goury, T.-M. Guerra, and C. Duriez, "Dynamic control of soft robots," in *Proc. Int. Conf. Soft Robot. World Congress*, 2017, pp. 46–53.

[5] C. Della Santina, R. K. Katzschmann, A. Bicchi, and D. Rus, "Model-based dynamic feedback control of a planar soft robot: Trajectory tracking and interaction with the environment," *Int. J. Robot. Res.*, 2019, doi: 10.1177/0278364919897292.

[6] G. Runge and A. Raatz, "A framework for the automated design and modelling of soft robotic systems," *CIRP Ann.*, vol. 66, no. 1, pp. 9–12, 2017.

[7] B. Kim, J. Ha, F. C. Park, and P. E. Dupont, "Optimizing curvature sensor placement for fast, accurate shape sensing of continuum robots," in *Proc. IEEE Int. Conf. Robot. Autom.*, 2014, pp. 5374–5379.

[8] B. A. Jones and I. D. Walker, "Kinematics for multisection continuum robots," *IEEE Trans. Robot.*, vol. 22, no. 1, pp. 43–55, Feb. 2006.

[9] H. Wang, B. Yang, Y. Liu, W. Chen, X. Liang, and R. Pfeifer, "Visual servoing of soft robot manipulator in constrained environments with an adaptive controller," *IEEE/ASME Trans. Mechatronics*, vol. 22, no. 1, pp. 41–50, Feb. 2017.

[10] V. Falkenhahn, A. Hildebrandt, R. Neumann, and O. Sawodny, "Model-based feedforward position control of constant curvature continuum robots using feedback linearization," in *Proc. IEEE Int. Conf. Robot. Autom.*, 2015, pp. 762–767.

[11] C. Della Santina, R. K. Katzschmann, A. Bicchi, and D. Rus, "Dynamic control of soft robots interacting with the environment," in *Proc. IEEE Int. Conf. Soft Robot.*, 2018, pp. 46–53.

[12] R. K. Katzschmann, C. Della Santina, T. Yasunori, A. Bicchi, and D. Rus, "Dynamic motion control of multi-segment soft robots using piecewise constant curvature matched with an augmented rigid body model," in *Proc. IEEE Int. Conf. Soft Robot.*, 2019, pp. 454–461.

[13] F. Renda, F. Boyer, J. Dias, and L. Seneviratne, "Discrete cosserat approach for multisection soft manipulator dynamics," *IEEE Trans. Robot.*, vol. 34, no. 6, pp. 1518–1533, Dec. 2018.

[14] W. S. Rone and P. Ben-Tzvi, "Continuum robot dynamics utilizing the principle of virtual power," *IEEE Trans. Robot.*, vol. 30, no. 1, pp. 275–287, Feb. 2014.

[15] S. Grazioso, G. Di Gironimo, and B. Siciliano, "A geometrically exact model for soft continuum robots: The finite element deformation space formulation," *Soft Robot.*, vol. 6, no. 6, pp. 790–811, 2019.

[16] H. Sadati *et al.*, "TMTDyn: A matlab package for modeling and control of hybrid rigid-continuum robots based on discretized lumped system and reduced order models," *Int. J. Robot. Res.*, 2019, doi: 10.1177/0278364919881685.

[17] M. W. Hannan and I. D. Walker, "Kinematics and the implementation of an elephant's trunk manipulator and other continuum style robots," *J. Field Robot.*, vol. 20, no. 2, pp. 45–63, 2003.

[18] R. J. Webster III and B. A. Jones, "Design and kinematic modeling of constant curvature continuum robots: A review," *Int. J. Robot. Res.*, vol. 29, no. 13, pp. 1661–1683, 2010.

[19] U. M. Ascher and L. R. Petzold, *Computer Methods for Ordinary Differential Equations and Differential-Algebraic Equations*, vol. 61. Philadelphia, PA, USA: SIAM, 1998.

[20] B. Siciliano, L. Sciavicco, L. Villani, and G. Oriolo, *Robotics: Modelling, Planning and Control*. Berlin, Germany: Springer Science & Business Media, 2010.

[21] C. Della Santina and D. Rus, "Control oriented modeling of soft robots: the polynomial curvature case," *IEEE Robot. Autom. Lett.*, vol. 5, no. 2, pp. 290–298, Apr. 2020.